PORT SAID ENGINEERING RESEARCH JOURNAL

Faculty of Engineering - Port Said University
Volume 29 No. 1 pp: 81:91

Triband Voltage Doubler Based Efficient Rectifying Circuit for Energy Harvesting

Rania M. Abdallah [1], Ahmed A. Eid [2], Heba Y. Soliman [3]

[1] *Electrical Engineering Department, Faculty of Engineering, Port Said University, Port Said, Egypt, email: eng_rania99@eng.psu.edu.eg*

[2] *Electrical Engineering Department, Faculty of Engineering, Port Said University, Port Said, Egypt, email: eidahmed26@hotmail.com*

[3] *Electrical Engineering Department, Faculty of Engineering, Port Said University, Port Said, Egypt, email: hebayms@eng.psu.edu.eg*

**Corresponding author, DOI: 10.21608/PSERJ.2024.319422.1366*

Received 8-9-2024
Revised 5-10-2024
Accepted 3-11-2024

ABSTRACT

This paper proposes an efficient triband rectifying circuit based on the Schottky diode for energy harvesting applications. Using a new compact impedance matching network, the rectifying circuit is matched at the GSM 1800, UMTS 2100, and WiFi 2450 bands. The design uses a substrate of Rogers Duroid 5880 with a thickness of 1.575 mm and ε_r=2.2. High Power Conversion Efficiency (PCE) is achieved in the rectifying circuit by using a microstrip DC pass filter for fundamental and second harmonic rejection. With a 2.8 KΩ circuit load and an input power of 0 dBm, the simulated efficiencies obtained at the GSM 1800, UMTS 2100, and WiFi 2450 bands are 45%, 19%, and 58.5%, respectively. For an input Radio Frequency (RF) power of -5 dBm, the efficiencies obtained are 49%, 38%, and 50 %, respectively, at a load resistance of 2.8 KΩ using an ADS simulator. There are numerous applications for the proposed triband rectifying circuits, which can power low-power sensors and electronic devices.

Keywords: Energy harvesting, Harmonic filters, Impedance matching, Rectennas, Rectifiers.

1 INTRODUCTION

Most portable electronic devices use batteries as a power source which has several drawbacks. These include increased weight and size as well as the requirement for periodic maintenance because of the short battery life, which can be challenging and costly depending on the environmental conditions [1-4]. Various energy sources can power IoT (Internet of Things) sensors and devices. Since Radio Frequency (RF) energy sources are renewable and always available, they are gaining popularity among all available possibilities [5-7]. Powering up low-power electronic devices using Radio Frequency Energy Harvesting (RF-EH) eliminates the need for a battery, resulting in a reduction in the device's cost, weight, and size. The rectenna, which is made up of two main blocks, is the essential component of RF-EH, as shown in Fig. 1. The first is the antenna, which transforms RF energy into an RF signal. The rectifying circuit, which is the second block, transforms the RF signal into a DC voltage that powers an electronic device [8].

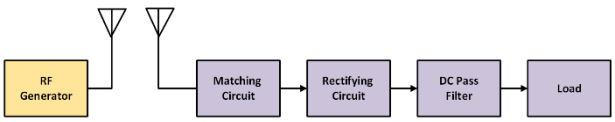

Figure 1: Block schematic of rectenna for ambient RF-EH.

In practice, the majority of reported rectennas are not suited to the levels of ambient signal [9]. The input power levels utilized in the designs were considerably higher than the levels of the surrounding ambient input power. Field measurements are necessary to ascertain the power density and frequency range of the surrounding wireless radiation. From the field measurements in [10, 11] and predictions based on calculations in [12] it was found that the average received power varies from -30 dBm to -10. Mobile power levels in various frequency bands, as shown in Table 1, are typically one to two orders of magnitude lower than the levels of power

received at the Base Station (BS). Table 1 shows that the frequency bands WiFi 2450, GSM1800, GSM 900, and 3G have the highest average power of –17.7, –15.3, –21.2, and –22.5 dBm, respectively. For optimal performance, the RF harvester should therefore be placed in a strategic location close to BSs.

Broadband, dual-band, multi-band, and single-band frequencies are all possible for RF-EH applications. A narrow-band rectenna offers higher power conversion efficiency (PCE) at low power levels, whereas a multi-band rectenna can collect more power but has a lower PCE [13]. The best solution is to develop a dual-band or multi-band rectenna that maximizes PCE at frequencies with the strongest ambient signals. However, most designs utilize input power levels that exceed the actual RF energy found in ambient environments.

Table 1. Various public telecommunication bands' measured ambient power densities [10].

Frequency Band	Operating Frequency (GHz)	Average Power Received (dBm)
GSM 900 (MTX)	0.88 - 0.915	-27.8
GSM 900 (BTX)	0.925 - 0.960	-21.2
GSM 1800 (MTX)	1.710 - 1.785	-42.7
GSM 1800 (BTX)	1.805 - 1.880	-15.3
3G (MTX)	1.920 - 1.980	-26.7
3G (BTX)	2.110 - 2.170	-22.5
ISM 2400	2.305 - 2.400	-30.1
WiFi 2450	2.400 - 2.500	-17.7

The paper's remaining sections are arranged as follows. The design of an improved triband rectifying circuit with harmonics-rejection is described in section 2. Section 2.1 describes the simulation results and performance evaluation of the triband rectifying circuit. In section 2.2, conclusions are finally drawn.

2. RECTIFYING CIRCUIT DESIGN

Since the rectifying circuit determines the effectiveness of the RF to DC power conversion, it is a crucial component of a rectenna. The merits of an evaluation vary based on the application. However, benchmarks for comparison are established for essential parameters including output power, sensitivity, and PCE. Additionally, in addition to these benefits, other manufacturing auxiliary elements such as low cost, fabrication process maturity, and availability of bulk production are also critical. RF-DC conversion efficiency is given by [14]:

$$\eta_{RF-DC} = \frac{P_{out}}{P_{RF}} \quad (1)$$

$$P_{out} = \frac{V_{out}^2}{R_L} \quad (2)$$

Where R_L is the load resistance, P_{RF} is the incident RF signal power, P_{out} is the output power, and V_{out} is the output voltage.

Figure 2 illustrates that the rectenna, a nonlinear element, consists of three components; a receiving antenna, a matching network, and a load. The total efficiency of the rectenna reflects the efficiency of each component, as shown in Fig. 2. The total rectenna efficiency η_T can be expressed as [15, 16]

$$\eta_T = \eta_a . \eta_m . \eta_o . \eta_p . \eta_{tr} \quad (3)$$

Where η_a is the efficiency of the receiving antenna, η_m is the matching network efficiency, η_{tr} is the dc source-to-load transfer process efficiency, η_o the nonlinear PCE and η_p is the parasitic efficiency.

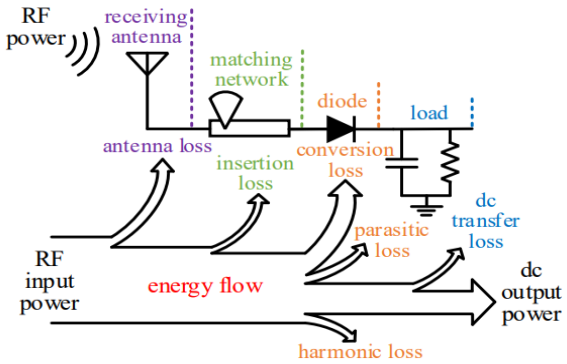

Figure 2: The loss mechanism in rectenna [16].

The harvester's sensitivity is a crucial parameter that significantly affects rectenna performance. Sensitivity refers to the power threshold at which the rectifier can harvest RF energy, depending on the diode's turn-on (threshold) voltage, Vth, which is the voltage needed for the diode to be forward-biased [17]. Lowering the turn-on threshold voltage increases energy PCE at a given power, meaning the rectifier becomes more sensitive. Unfortunately, previous research has overlooked the importance of the harvester's sensitivity. It can be expressed as [18].

$$Sensitivity\ (\mathrm{dBm}) = \log_{10}\left(\frac{\mathrm{P}}{1\mathrm{mW}}\right) \quad (4)$$

where P is the minimum power required by the system to perform the task. The output power of the RF energy harvester is the DC power that is determined by V_{out} and I_{load} across the load resistance R_L. The significance of V_{out} and I_{load} fluctuates based on the load conditions. In the context of the RF energy harvester, the significance of V_{out} outweighs that of I_{load} when the sensor functions as a load at the output. However, in applications such as LED or electrolysis, I_{load} takes precedence over V_{out} [19]. The most advanced low-power sensor available today would require a 10 µA DC current and a DC voltage source of about 1 V. When constructing an energy harvester to supply power to an electronic circuit, it is

necessary to indicate the DC output power. However, when evaluating RF energy harvesters for distant sensors, it is essential to separately define the output voltage and current. While the literature extensively discusses efficiency, its actual application in ambient RF-EH may have limitations. This is because a remote sensor's specific voltage and input current requirements can prohibit the sensor from being energised, even though an RF harvester could be able to deliver an output DC power higher than what the sensor needs [20]. Robust power handling capabilities, low power consumption, and strong power sensitivity are essential characteristics of a good rectifier [21].

2.1 Rectifying Circuit Topology

There are numerous rectifier topologies that can be employed, including Greinacher, half wave, voltage doubler, and shunt diode rectifiers. Although the single series topology has a minimal biassing need, its limited power handling capabilities due to its low breakdown voltage will negatively impact broadband performance. Additionally, its narrow bandwidth is its main drawback. Charge pump rectifiers with two or more diodes are examples of multi-diode rectifiers that can be utilized to increase power handling capabilities [22].

Due to its sensitivity, simplicity, output voltage, and high efficiency voltage doubler rectifying circuit is the best choice for many rectenna designers. The voltage doubler's high sensitivity may eliminate the need for extra boost converter circuitry, simplifying the system [23].

In this work, a voltage-doubler rectifier topology, shown in Fig. 3, is adopted [24]. Voltage doubler rectifying circuit can be analyzed into two stages, stage 1 is a clamping circuit consisting of capacitor C1 and shunt diode D1 used to shift the DC level of signal whereas stage 2 is a peak detector circuit that holds the output voltage at the peak value. It consists of a series diode D2 followed by a shunt capacitor C2. The output voltage (V_{out}) is calculated by using the following equations [25].

$$V_{C1} = V_{in} - V_{TH1} \quad (5)$$

$$V_{out} = 2V_{in} - V_{TH1} - V_{TH2} \quad (6)$$

Where Vc_1 is the voltage applied across the capacitor C1, V_{TH1} and V_{TH2} are the threshold voltages of diodes D1 and D2 respectively.

For two identical diodes with threshold voltage V_{TH} The output voltage (V_{out}) can be expressed as

$$V_{out} = 2V_{in} - 2V_{TH} \quad (7)$$

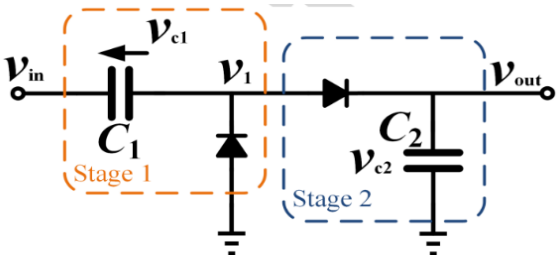

Figure 3: Voltage doubler rectifying circuit [24].

2.2 Diode Selection

The diode, which is the primary rectifying component in the RF-EH, has a big impact on how well the rectifying circuit works [26]. Therefore, selecting the appropriate diode is crucial. The series resistance, junction capacitance, breakdown voltage, and threshold voltage are important factors to consider while choosing a diode. The threshold voltage, Vth, affects PCE and rectifier sensitivity, while the breakdown voltage, Vbr, sets the rectifier's power handling limit; output voltage must not exceed Vbr. A higher Vbr allows for greater input power but results in an increased Vth, reducing RF PCE. Series resistance, Rs, caused by charge movement within the semiconductor, enables higher PCE at lower powers but limits performance at higher power levels. Junction capacitance, Cj, constrains the maximum operating frequency, necessitating diodes with lower Cj for higher frequency applications. The diode cutoff frequency can be calculated using Eq. 8. [27]. Due to the regulations on the ambient RF signals' maximum power levels, they are always available at very low power levels. For the design of sensitive and efficient RF to DC rectification circuits diodes with lower Vth should be used. In Table 2 many commercially available Schottky diodes with their parameters were shortlisted [28].

$$\omega_c = 2\pi f_c = \frac{1}{R_s C_j} \quad (8)$$

Where $\omega_c$is the diode cut off frequency in radian and f_c is the diode cut off frequency in Hertz.

The diode with minimum threshold voltage is SMS-7630 so it was selected as a rectifying element in this work. Spice model SMS 7630 is shown in Fig. 4 and its parameters are listed in Table 3.

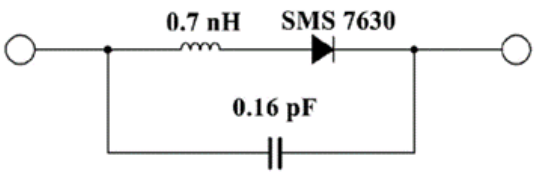

Figure 4: The SMS 7630 Schottky diode's spice model [29, 30].

Table 2. Different Schottky diode parameters [28].

Diode	Vth (V)	Vb (V)	Rs (Ω)	Cj (pF)
HSMS 2862	0.65	7	6	0.18
HSMS 8202	0.35	4	14	0.26
SMS 7630	0.34	2	20	0.14
SMS 7621	0.55	3	12	0.1
MA 40417	0.65	11	4.9	0.04

In a realistic PN-junction diode, the net current I through the junction for a bias voltage V is [32]

$$I = I_0\left(e^{V/nV_{th}} - 1\right) \tag{9}$$

Where I_0 is the reverse current, n is the ideality factor which is constant (ranging from 1 to 2) and the thermal voltage Vth equal k_BT/q where k_B is the Boltzmann constant, q is the electron charge and T is the absolute temperature. At 300 K, the average thermal voltage is 25.85 mV. As noted in Eq. 9, A PN junction diode's current saturates at I_o under reverse bias, but it grows exponentially with forward bias voltage V. Using the Taylor series expansion, Eq. 9 can be expressed as [32].

$$I = I_0\left(\frac{V}{nV_{th}} + \frac{1}{2!}\frac{V^2}{n^2V_{th}^2} + \frac{1}{3!}\frac{V^3}{n^3V_{th}^3} + \frac{1}{4!}\frac{V^4}{n^4V_{th}^4} + \frac{1}{5!}\frac{V^5}{n^5V_{th}^5}\ldots\right) \tag{10}$$

2.3 DC Pass Filter

A DC pass filter is necessary for harmonic rejection, as harmonics are generated during RF to DC rectification due to diode non-linearity in the rectifying circuit [33, 34]. Electrical filters are employed to select or suppress specific frequency bands, typically using passive components like capacitors and inductors [35]. While passive lumped-element filters perform well at low frequencies, they have two issues when applied at higher RF and microwave frequencies: difficulties when applying them at microwave frequencies and restricted availability of inductor and capacitor values.

To simulate ideal lumped parts, distributed components like transmission line stubs that are either open or short-circuited are frequently utilized. Furthermore, the distances between filter components are not insignificant at microwave frequencies [36].

Benefits of microstrip filters include their low cost, portability, and simplicity of usage. Bandstop filters (BSFs) are essential components in modern RF/microwave communication systems [37]. Their main function is to allow desired signals to pass while blocking undesired ones. A traditional microstrip BSF features quarter-wavelength shunt open-circuited resonators connected by quarter-wavelength lines. Figure 5 illustrates one section of a conventional distributed microstrip BSF [38]. Varying the characteristic impedances of the connecting lines can improve the performance of quarter-wave resonator filters.

Rather of using a rectangular quarter-wave stub, MRS provides efficient wideband harmonic suppression [39, 40]. For the second and third harmonics of 2.14 GHz, we fabricated one MRS and one standard quarter-wave stub. Figure 6 compares the measured results. The insertion loss for the 2nd and 3rd harmonics is better than 38.37 dB and 29.53 dB, respectively. In the 200 MHz bandwidth region of MRS at a center frequency of 4.28 GHz, the insertion loss for the 3rd harmonic exceeds 28 dB, while in its 300 MHz bandwidth region, the insertion loss exceeds 26 dB [41]. Figure 7 shows how to model the radial stub as a series combination of a capacitor and an inductor [42]. The values for Z_{in}, L_{rs}, and C_{rs} can be calculated using Eqs. 11, 12, and 13, respectively [43].

Table 3. SMS 7630 Schottky diode parameters [31].

Is = 5E-6 A	M = 0.4	BV =2 V	NBVL =1
Rs = 30 Ω	EG =0.69	IBV = 1e-4	TNOM = 27C
N = 1.05	EV	ISR = 0 A	FFE = 1
TT = 1E-11 S	XTI = 2	NR = 2	
Cjo = 1.4E-13 F	KF = 0	NBV =1	
Vj = 0.34 V	Af = 1	IBVL = 0 A	
	Fc = 0.5		

$$Z_{in} = -j\frac{120\pi h\beta}{\theta_r\sqrt{\varepsilon_{eff}}}\left(ln\frac{r_i}{r_o} + \frac{1}{2} + \frac{2}{(\beta r_o)^2}\right) \tag{11}$$

$$L_{rs} = \frac{120\pi h}{\theta_r c}\left[ln\frac{r_o}{r_i} - \frac{1}{2}\right] \tag{12}$$

$$C_{rs} = \frac{\theta_r r_o^2 \varepsilon_{eff}}{240\pi hc} \tag{13}$$

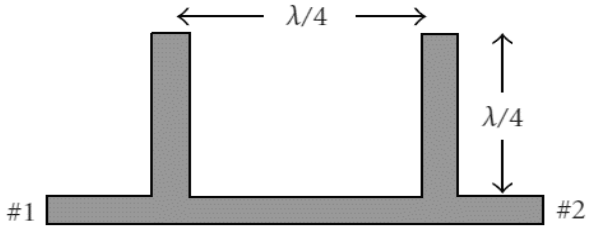

Figure 5: Conventional distributed microstrip BSF [38].

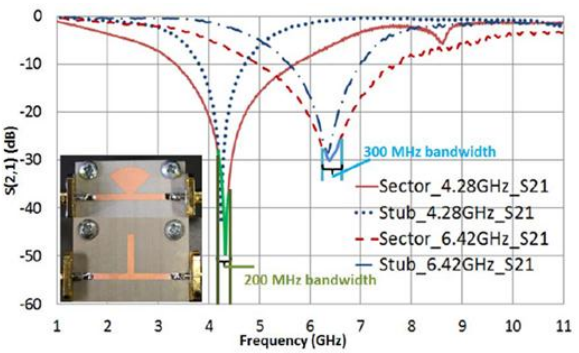

Figure 6: Insertion loss of MRS and one quarter-wave stub [41].

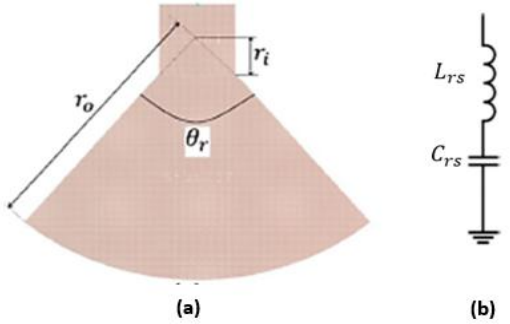

Figure 7: Equivalent circuit model of radial stub [42].

where c is the speed of light, ε_{eff} is the effective dielectric constant, r_i and r_o are the inner and outer radial stubs, β is the phase constant, θ_r is the spanning angle in radians, and h is the dielectric thickness. To achieve a sufficient frequency bandwidth, these stubs are cascaded [44]. However, this method has the drawback of increasing the circuit size. Figure 8 depicts a typical two-stub radial resonator.

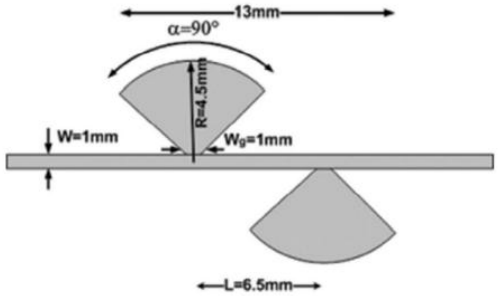

Figure 8: Typical two-stub radial resonator [44].

Table 4. Geometrical parameters of the proposed rectifier.

Parameter	Width/ Length (mm)	Parameter	Width/ Length (mm)	Parameter	Width1/ Width2/ Length (mm)
TL1	10.956/ 14.2608	TL5	2.00041/ 14.8599	TAP1	8.98749/ 9.14848/ 27.8053
TL2	10.95/ 21.0209	TL6	2.04328/ 8.67394	TAP2	14.9833/ 11.1055/ 23.2089
TL3	9.7326/ 15.2173	TL7	2.00008/ 11.5178		
TL4	2.0227/ 10.0931	TL8	14.8046/ 16.0715		

In this work, the designed DC pass filter (output filter) consists of dual radial stubs. The optimized dimensions were found using ADS optimization tool.

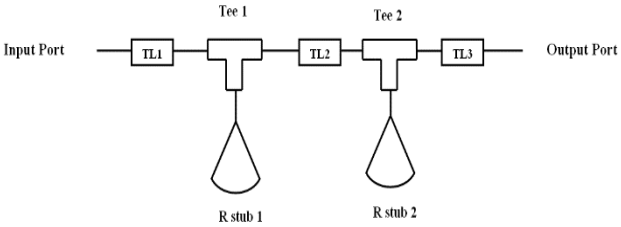

Figure 9: Topology of the DC pass filter.

In Fig. 10, the |S21| of the dc-pass filter is plotted against the frequency. It shows that the |S21| remains below −20 dBm within the frequency band of 1.8 GHz to 5.4 GHz. This indicates that the 1.8 GHz band's fundamental frequency, second order, and third order harmonics are all successfully eliminated by the filter. It also efficiently eliminates the second order harmonics and the fundamental frequency in the 2.4 GHz and 2.1 GHz regions.

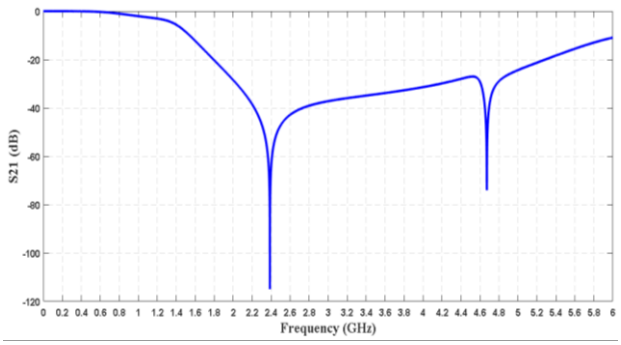

Figure 10: Simulated S21 of DC pass filter.

2.4 Impedance Matching

An impedance-matching network must be used in order for the receiving antenna to provide the maximum amount of power to the load [45]. The diodes in the rectifying circuit introduce nonlinearity, causing the input impedance of the circuit to be nonlinear. The output load value and the operating frequency of the input power both affect this nonlinearity.

This paper proposes a novel triple-band matching network to overcome the difficulties caused by the input impedance's nonlinearity [46].

The matching network is implemented using microstrip technology. It consists of a tapered line followed by two branch short-circuit stubs. To determine the ideal final values, Keysight Advanced Design System (ADS) multivariable multi-goal optimisation was used. Figure 11 shows the dual-band rectifier's schematic diagram. The geometrical parameters are listed in Table 4. The simulation results for |S11| at five different input power levels (0, -5, -10, -15, and -20 dBm) are presented in Fig. 12. The simulation results demonstrate a wide bandwidth for the WiFi, GSM 1800, and UMTS 2100 bands across a range of low input power levels.

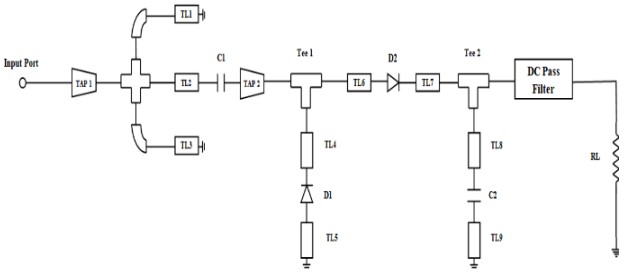

Figure 11: The proposed topology for the rectifying circuit consists of an impedance-matching network of two branches.

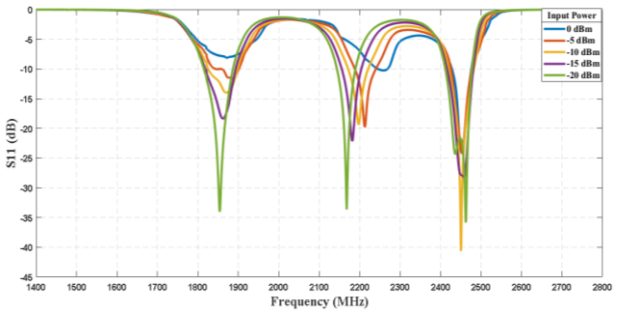

Figure 12: Simulated S11 of the proposed rectifier at five power levels with R_L = 2.8 kΩ.

3. SIMULATION RESULTS

One of the rectifier's performance metrics is its RF-to-DC efficiency. The frequency and input power have a nonlinear relationship with the efficiency. Figure 13 shows the PCE versus frequency simulation results. For single tone simulation the efficiency achieved at zero dBm input power and 2.8 kΩ load resistance is 45% ,19%, and 58.5% at 1860 MHz and 2450 MHz, respectively. At -5 dBm power level and 2.8 kΩ load resistance is 49%, 38%, and 50 % at 1860 MHz, 2150 MHz and 2450 MHz, respectively. At -10 dBm power level and 2.8 kΩ load resistance is 40%, 30% and 38 % at 1860 MHz, 2150 MHz and 2450 MHz, respectively. At -15 dBm power level and 2.8 kΩ load resistance is 31%, 25% and 25 % at 1860 MHz, 2150 MHz and 2450 MHz, respectively.

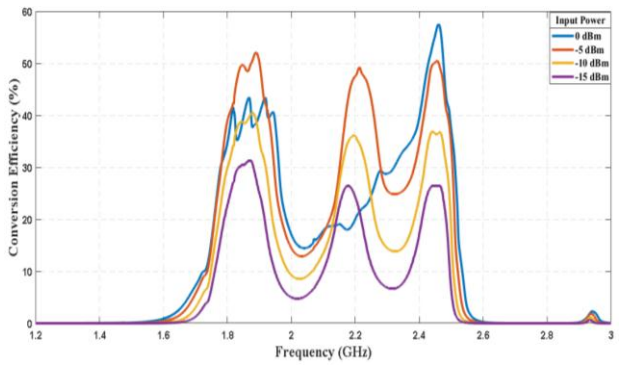

Figure 13: Simulated rectifier conversion efficiency as a function of frequency at five input power levels for R_L=2.8 kΩ.

The relationship between the input power and the output voltage is displayed in Fig. 14, which is the result of the simulation. It is clear that the output voltage is 0.7 volts at 1860 MHz, 1.1 volts at 2150 MHz, and 1.28 volts at 2450 MHz with an input power of 0 dBm and a load resistance of 2.8 kΩ. Additionally, the PCE is non-linear and depends on the load resistance R_L.

With an input frequency of 1840 MHz, Figs. 15 and 16 depict the simulated PCE and output DC voltage of the proposed rectifying circuit for a range of RL values (100 Ω to 20 kΩ) at five input power levels. The simulated output DC voltage and efficiency for various RL values ranging from 100 Ω to 20 kΩ for five distinct input power levels at an input frequency of 2150 MHz are shown in Figs. 17 and 18, respectively. The simulated output DC voltage and efficiency for various RL values ranging from 100 Ω to 20 kΩ for five distinct input power levels at an input frequency of 2450 MHz are shown in Figs. 19 and 20, respectively.

It is shown that the total number of tones and the uniform spacing between several tones can be used to increase the RF-to-DC efficiency when they are weighted equally [47].

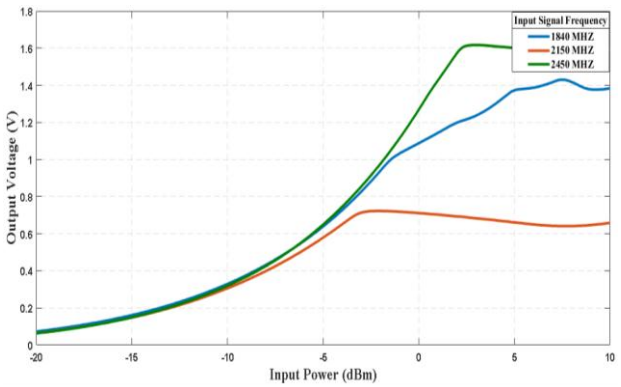

Figure 14: Simulated rectifier output voltage vs. input power at three different frequencies for R_L =2.8 kΩ.

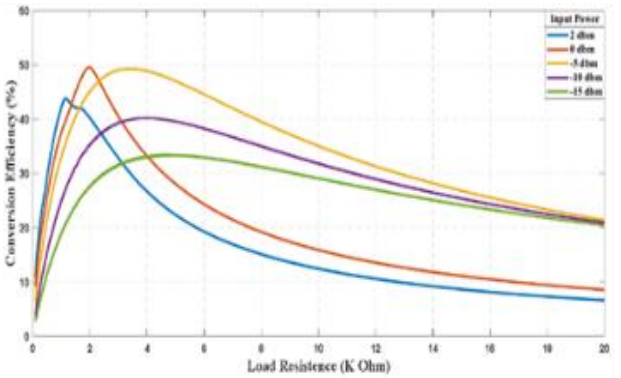

Figure 15: The conversion efficiency vs. R_L for five different input power levels at 1840 MHz.

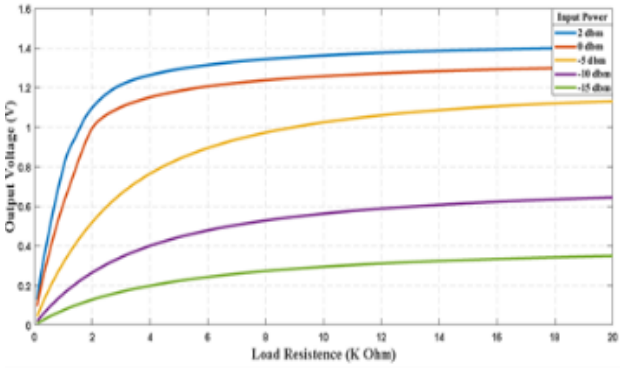

Figure 16: The output voltage vs. R_L for five different input power levels at 1840 MHz.

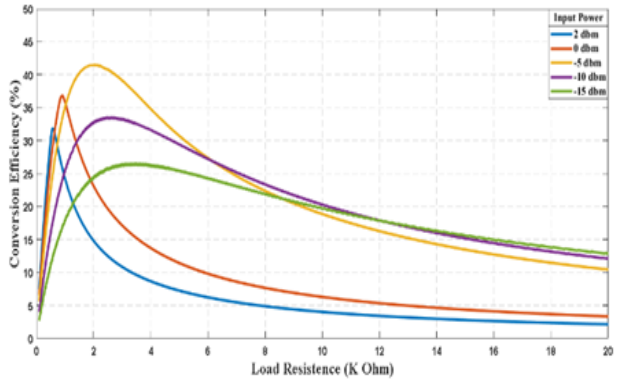

Figure 17: The conversion efficiency vs. R_L for five input power levels at 2150 MHz.

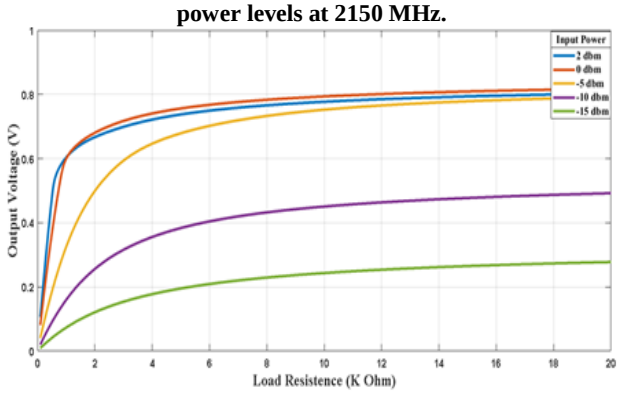

Figure 18: The output voltage vs. R_L for five input power levels at 2150 MHz.

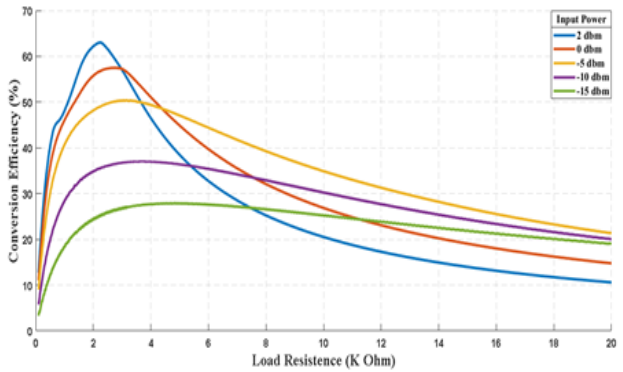

Figure 19: The conversion efficiency vs. R_L for five input power levels at 2450 MHz.

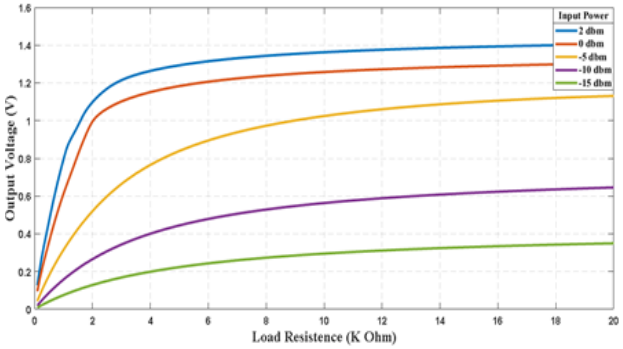

Figure 20: The output voltage vs. R_L for five input power levels at 2450 MHz.

For multi-tone input signals with input power of -15 dBm for each tone (1-tone at 2450 MHz, 2-tone at 2440 and 2450 MHz, 3-tone 2-tone at 2440, 2450, 2460 MHz, and 4-tone with 10 MHz-spacing from 2440 to 2470 MHz), Fig. 21 shows the simulated RF-to-DC PCE of the proposed rectifier vs. load resistance.

The maximum efficiency rises from 25% for the single tone at 2450 MHz to 35% for the 3-tone signal at 2440, 2450, and 2460 MHz and 38% for the 4-tone signal at 2440, 2450, 2460, and 2470 MHz when the power level of each tone is -15 dBm, as illustrated in Fig. 21.

Figures 22 and 23 depict, respectively, the simulated RF-to-DC efficiency corresponding to a single tone at 2450 MHz, dual-tone at 1840 and 2450 MHz, and triple-tone at 1840, 2150, and 2450 MHz at input powers of -10 dBm and -15 dBm for each tone.

As indicated in Table 5, the rectifying circuit's performance is assessed by comparison with analogous prior studies.

Most of the work has been done for a single band, and some works have been done for multiband, but they were designed and optimized at input power levels much higher than the available RF power. The proposed rectifying circuit operates efficiently at relatively low input power levels.

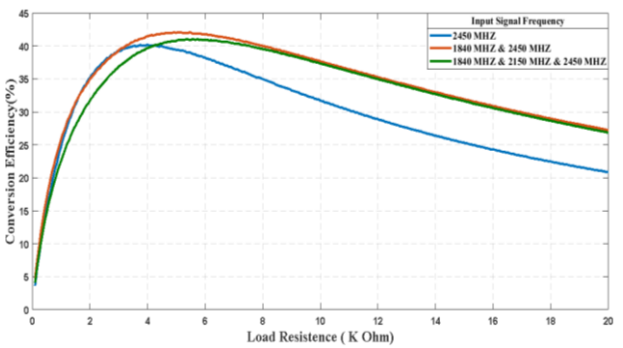

Figure 21: Simulated conversion efficiency vs. R_L for multi-tone input signals with input power of -15 dBm for each tone.

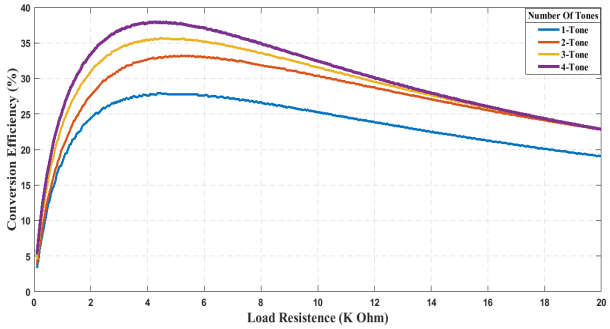

Figure 22: Simulated conversion efficiency vs. R_L for multi-tone input signals with input power of -10 dBm for each tone.

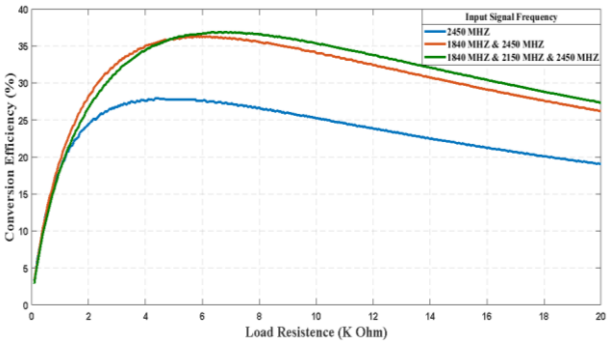

Figure 23: Simulated conversion efficiency vs. R_L for multi-tone input signals with input power of -15 dBm for each tone.

Most researchers study the performance of rectenna at relatively high input power values (greater than or equal to 0 dBm) as observed in Table 5 focusing on achieving high conversion efficiency regardless that they study the performance at high input power compared to the Actual measured RF Power in the environment as illustrated in Table 1. The work in [59] studies the Performance of rectenna designed to operate at 1.8 GHz and 2.45 GHz bands respectively for an input power of 3dBm and 4dBm, also the work in [60] studies the performance of rectenna designed to operate at 5.8 GHZ with an input power of 16.7 dBm which is very high input power. For a multiband antenna achieving high Efficiency at low input power is very challenging as shown in [61] at 2.1 GHz and a 1500 Ω load with an input power of −10 dBm The CE was observed to be only 7 %. As shown in this work the Performance of the proposed triband rectenna was studied at multiple input power values, it's obvious that the achieved conversion efficiency at low input power values is higher than results in [48] at the cost of larger size and higher design complexity.

Table 5. Comparison between related designs and the proposed rectifying circuit.

Reference	Rectifying circuit Topology	Diode Type	Frequency band	PCE (%) at Pin dBm input power		Maximum PCE
				-15	-10	
[48]	Single series diode	HSMS 285B	0.9 GHZ 1.8 GHZ 2.1 GHZ	18 26 8	26 33 11	- 35% at 0 dBm -
[49]	Single series diode	HSMS-285B	0.9 GHZ 1.8 GHZ 2.1 GHZ	- - -	40 33 25	-
[50]	Voltage doubler	HSMS-2860	3.5 GHz	-		29.72 % at 6 dBm
[51]	Single series diode	BAT15 -03W	0.915 GHZ 2.45 GHZ	-		74% at 9 dBm 73% at 9 dBm
[52]	Three parallel volage doubler	HSMS-2852	0.9 GHZ 1.8 GHZ 2.45 GHZ	- - -	33.7 21.8 20	57.8% at 0 dBm 55.8% at 0 dBm 56.5% at 0 dBm
[53]	Single series diode	SMS76 30	2.4 GHZ 3.5 GHZ	- -	42.1 42.5	59.8 % at 0 dBm 56.3 % at 0 dBm
[54]	Voltage doubler	HSMS 2850	0.9 GHZ	-		43.6% at 0 dBm 50.2 % at 2 dBm
[55]	Voltage doubler	HSMS 2852	2.45 GHZ	-	37	67% at 0 dBm
[56]	Voltage doubler	SMS-7630	2.45 GHZ 5.8 GHZ	- -	50.7 20.1	57.1 % at 0 dBm 39.2 % at 0 dBm
[57]	Single shunt diode	SMS-7630	10 GHZ	-	≈ 8	34 % at 7 dBm
	Voltage doubler				≈ 8	43 % at 6 dBm
[58]	Voltage doubler	HSMS 285C	0.9 GHZ	-	-	45.9% at -10 dBm
Proposed topology	Voltage doubler	SMS76 30-079	1.8 GHZ 2.1 GHZ 2.4 GHZ	31 25 25	40 30 38	45% at 0 dBm 19% at 0 dBm 58.5% at 0 dBm

4. CONCLUSION

In this study, we have proposed Triband rectifying circuits that can operate at GSM 1800, UMTS 2100, and WiFi 2450 bands and can power low-power electronic devices. We selected the RT/Duroid 5880 as the substrate for this purpose. For the design, the SMS7630-079 diodes were selected. The IMN network was designed using commercial software. When the input power becomes 2 dBm and the output load is 2.4 KΩ, our solution achieves a maximum PCE of 63%. In low-power scenarios, our suggested design performs as well as or better than other comparable designs found in the literature.

5. REFERENCES

[1] C. Song, P. Lu and S. Shen, "Highly Efficient Omnidirectional Integrated Multiband Wireless Energy Harvesters for Compact Sensor Nodes of Internet-of-Things," in IEEE Transactions on Industrial Electronics, vol. 68, no. 9, pp. 8128-8140, Sept. 2021. DOI: 10.1109/TIE.2020.3009586.

[2] C. Song, Y. Huang, J. Zhou, J. Zhang, S. Yuan and P. Carter, "A High-Efficiency Broadband Rectenna for Ambient Wireless Energy Harvesting," in IEEE Transactions on Antennas and Propagation, vol. 63, no. 8, pp. 3486-3495, Aug. 2015. DOI: 10.1109/TAP.2015.2431719.

[3] S. M. K. Azam, Md. Shazzadul, A. K., and M. Othman, "Monopole Antenna on Transparent Substrate and Rectifier for Energy Harvesting Applications in 5G," International Journal of Advanced Computer Science and Applications, vol. 11, no. 8, 2020.

[4] S. Kim et al., "Ambient RF Energy-Harvesting Technologies for Self-Sustainable Standalone Wireless Sensor Platforms," in Proceedings of the IEEE, vol. 102, no. 11, pp. 1649-1666, Nov. 2014. DOI: 10.1109/JPROC.2014.2357031.

[5] A. Bakytbekov, T. Q. Nguyen, C. Huynh, K. N. Salama, and A. Shamim, "Fully printed 3D cube-shaped multiband fractal rectenna for ambient RF energy harvesting," Nano Energy, vol. 53, pp. 587–595, 2018. DOI: 10.1016/j.nanoen.2018.09.022.

[6] L.-G. Tran, H.-K. Cha, and W.-T. Park, "RF power harvesting: a review on designing methodologies and applications," Micro Nano Syst. Lett., vol. 5, no. 1, 2017. DOI: https://doi.org/10.1186/s40486-017-0051-0.

[7] D. K. Ho, V.-D. Ngo, I. Kharrat, T. P. Vuong, Q. C. Nguyen, and M. T. Le, "A novel dual-band rectenna for ambient RF energy harvesting at GSM 900 MHz and 1800 MHz," Adv. Sci. Technol. Eng. Syst. J., vol. 2, no. 3, pp. 612–616, 2017. DOI:10.25046/aj020378.

[8] M. Cansiz, D. Altinel, and G. K. Kurt, "Efficiency in RF energy harvesting systems: A comprehensive review," Energy (Oxf.), vol. 174, pp. 292–309, 2019. DOI: https://doi.org/10.1016/j.energy.2019.02.100.

[9] F. Khalid, W. Saeed, N. Shoaib, M. U. Khan, and H. M. Cheema, "Quad-Band 3D Rectenna Array for Ambient RF Energy Harvesting," International Journal of Antennas and Propagation, vol. 2020, p. e7169846, May 2020, doi: 10.1155/2020/7169846.

[10] M. Piñuela, P. D. Mitcheson and S. Lucyszyn, "Ambient RF Energy Harvesting in Urban and Semi-Urban Environments," in IEEE Transactions on Microwave Theory and Techniques, vol. 61, no. 7, pp. 2715-2726, July 2013. DOI: 10.1109/TMTT.2013.2262687.

[11] S. Muhammad et al., "Harvesting Systems for RF Energy: Trends, Challenges, Techniques, and Tradeoffs," Electronics, vol. 11, no. 6, p. 959, Mar. 2022. DOI: https://doi.org/10.3390/electronics11060959.

[12] O. M. AbdelGhany, A. G. Sobih, and A. M. El-Tager, "Outdoor RF spectral study available from cell-phone towers in sub-urban areas for ambient RF energy harvesting," IOP Conf. Ser. Mater. Sci. Eng., vol. 610, no. 1, p. 012086, 2019.

[13] H. H. Ibrahim et al., "Radio frequency energy harvesting technologies: A comprehensive review on designing, methodologies, and potential applications," Sensors (Basel), vol. 22, no. 11, p. 4144, 2022.

[14] M. M. Mansour and H. Kanaya, "Efficiency-enhancement of 2.45-GHz energy harvesting circuit using integrated CPW-MS structure at low RF input power," IEICE Trans. Electron., vol. E102.C, no. 5, pp. 399–407, 2019.

[15] S. K. Divakaran, D. D. Krishna, and Nasimuddin, "RF energy harvesting systems: An overview and design issues," Int. J. RF Microw. Comput-Aid. Eng., vol. 29, no. 1, p. e21633, 2019.

[16] X. Gu, S. Hemour, and K. Wu, "Far-field wireless power harvesting: Nonlinear modeling, rectenna design, and emerging applications," Proc. IEEE Inst. Electr. Electron. Eng., vol. 110, no. 1, pp. 56–73, 2022.

[17] P. N. Alevizos and A. Bletsas, "Sensitive and nonlinear far-field RF energy harvesting in wireless communications," IEEE Trans. Wirel. Commun., vol. 17, no. 6, pp. 3670–3685, 2018.

[18] P. C. Kar and M. A. Islam, "Design and performance analysis of a rectenna system for charging a mobile phone from ambient EM waves," Heliyon, vol. 9, no. 3, p. e13964, 2023.

[19] D. Khan et al., "A survey on RF energy harvesting system with high efficiency RF-DC converters," Journal of Semiconductor Engineering, vol. 1, no. 1, pp. 13–30, 2020.

[20] A. Nimo, University of Freiburg, Department of Microsystems Engineering - IMTEK. Laboratory for Electrical Instrumentation. Georges-Köhler-Allee 106, 79110 Freiburg, Germany, T. Beckedahl, T. Ostertag, and L. Reindl, "Analysis of passive RF-DC power rectification and harvesting wireless RF energy for micro-watt sensors," AIMS Energy, vol. 3, no. 2, pp. 184–200, 2015.

[21] S. Hemour et al., "Towards Low-Power High-Efficiency RF and Microwave Energy Harvesting," in IEEE Transactions on Microwave Theory and Techniques, vol. 62, no. 4, pp. 965-976, April 2014.

[22] S. D. Joseph, Y. Huang, and S. S. H. Hsu, "Transmission lines-based impedance matching technique for broadband rectifier," IEEE Access, vol. 9, pp. 4665–4672, 2021.

[23] M. Wagih, A. S. Weddell, and S. Beeby, "High-efficiency sub-1 GHz flexible compact rectenna based on parametric antenna-rectifier co-design," in 2020 IEEE/MTT-S International Microwave Symposium (IMS), 2020.
[24] S. Fan et al., "A 2.45-GHz Rectifier-Booster Regulator with Impedance Matching Converters for Wireless Energy Harvesting," IEEE Transactions on Microwave Theory and Techniques, vol. 67, no. 9, pp. 3833–3843, Sep. 2019, doi:10.1109/TMTT.2019.2910062.
[25] Q. Awais, Y. Jin, H. T. Chattha, M. Jamil, H. Qiang, and B. A. Khawaja, "A compact rectenna system with high conversion efficiency for wireless energy harvesting," IEEE Access, vol. 6, pp. 35857–35866, 2018.
[26] W. Saeed, N. Shoaib, H. M. Cheema, and M. U. Khan, "RF Energy Harvesting for Ubiquitous, Zero Power Wireless Sensors," International Journal of Antennas and Propagation, vol. 2018, pp. 1–16, 2018.
[27] E. Cobas and M. S. Fuhrer, "Microwave rectification by a carbon nanotube Schottky diode," Appl. Phys. Lett., vol. 93, no. 4, p. 043120, 2008.
[28] Mutee-Ur-Rehman, W. Ahmad, M. I. Qureshi and W. T. Khan, "A highly efficient tri band (GSM1800, WiFi2400 and WiFi5000) rectifier for various radio frequency harvesting applications," 2017 Progress in Electromagnetics Research Symposium - Fall (PIERS - FALL), 2017, pp. 2039-2044.
[29] K. Çelik and E. Kurt, "Design and implementation of a dual band bioinspired leaf rectenna for RF energy harvesting applications," International Journal of RF and Microwave Computer-Aided Engineering, vol. 31, no. 11, Aug. 2021.
[30] H. Vu Ngoc Anh, N. M. Thien, L. H. Trinh, T. Nguyen Vu, and F. Ferrero, "Compact Dual-Band Rectenna Based on Dual-Mode Metal-Rimmed Antenna," Electronics, vol. 9, no. 9, p. 1532, Sep. 2020.
[31] A. Benayad and M. Tellache, "A compact energy harvesting multiband rectenna based on metamaterial complementary split ring resonator antenna and modified hybrid junction ring rectifier," International Journal of RF and Microwave Computer-Aided Engineering, vol. 30, no. 2, Nov. 2019.
[32] S. Gambhir, Arvind, and M. Singh, "Intrinsic nonlinearity of a PN-junction diode and higher order harmonic generation," arXiv [physics.app-ph], 2018.
[33] M.-J. Nie, X.-X. Yang, and J.-J. Lu, "A Broadband Rectifing Circuit with high efficiency for microwave power transmission," Progress In Electromagnetics Research Letters, vol. 52, pp. 135–139, 2015.
[34] L. Shen and X. Yang, "A novel rectifier circuit operating at dual-frequencies of 1.8 GHz and 2.4 GHz," 2013 IEEE MTT-S International Microwave Workshop Series on RF and Wireless Technologies for Biomedical and Healthcare Applications (IMWS-BIO), 2013, pp. 1-3.
[35] A. Chirap and V. Popa, "Insertion loss measurement of a lowpass microwave filter manufactured on FR4 laminate," in 2016 International Conference on Development and Application Systems (DAS), 2016.
[36] D. M. Pozar, Microwave Engineering, 4th ed. Nashville, TN: John Wiley & Sons, 2012.
[37] R. K. Joshi and A. R. Harish, "A planar bandpass filter using butterfly radial stub," Microw. Opt. Technol. Lett., vol. 49, no. 8, pp. 1872–1875, 2007.
[38] M. A. S. Alkanhal, "Compact bandstop filters with extended upper passbands," Act. Passiv. Electron. Compon., vol. 2008, pp. 1–6, 2008.
[39] Y.-F. Tsao, J. Würfl, and H.-T. Hsu, "Bandwidth Improvement of MMIC Single-Pole-Double-Throw Passive HEMT Switches with Radial Stubs in Impedance-Transformation Networks," Electronics, vol. 9, no. 2, p. 270, Feb. 2020.
[40] Z. Wang and C.-W. Park, "Novel wideband high-efficiency high-power amplifier using microstrip radial stub for 4G communication systems," Microwave and Optical Technology Letters, vol. 56, no. 6, pp. 1412–1418, Mar. 2014.
[41] Zhebin Wang and Chan-Wang Park, "Novel wideband GaN HEMT power amplifier using microstrip radial stub to suppress harmonics," 2012 IEEE/MTT-S International Microwave Symposium Digest, 2012, pp. 1-3.
[42] S. R. Borjlu and M. S. Khadem, "Novel microstrip dual-band quad-section bandpass filter using radial stub for wireless communication," J. Electr. Eng. Technol., vol. 14, no. 3, pp. 1327–1333, 2019.
[43] P. K. Singh, A. K. Tiwary, and N. Gupta, "Design of radial microstrip band pass filter with wide stop-band characteristics for gps application," Prog. Electromagn. Res. C Pier C., vol. 59, pp. 127–134, 2015.
[44] R. Dehbashi, H. D. Oskouei, and K. Forooraghi, "A novel broad-band microstrip radial stub resonator used in bias-T application," Microw. Opt. Technol. Lett., vol. 48, no. 9, pp. 1766–1770, 2006.
[45] M. Wang, L. Yang, and Y. Shi, "A dual-port microstrip rectenna for wireless energy harvest at LTE band," AEU - International Journal of Electronics and Communications, vol. 126, p. 153451, Nov. 2020.
[46] C. Song et al., "A novel six-band dual CP rectenna using improved impedance matching technique for ambient RF energy harvesting," IEEE Trans. Antennas Propag., vol. 64, no. 7, pp. 3160–3171, 2016.
[47] K. Neophytou and M. A. Antoniades, "DC voltage boosting technique in radio frequency wireless power transfer systems utilising high PAPR digital modulations," IET Microwaves, Antennas &

Propagation, vol. 13, no. 14, pp. 2457–2463, Aug. 2019.
[48] O. Assogba, A. K. Mbodji, A. Bréard, A. K. Diallo, and Y. Duroc, “Tri-Band Rectenna Dedicated to UHF RFID, GSM-1800 and UMTS-2100 Frequency Bands,” Sensors, vol. 22, no. 9, p. 3565, May 2022.
[49] S. Shen, C.-Y. Chiu, and R. D. Murch, “A Dual-Port Triple-Band L-Probe Microstrip Patch Rectenna for Ambient RF Energy Harvesting,” IEEE Antennas and Wireless Propagation Letters, vol. 16, pp. 3071–3074, 2017.
[50] O. M. A. Dardeer, H. A. Elsadek, and E. A. Abdallah, “Compact Broadband Rectenna for Harvesting RF Energy in WLAN and WiMAX Applications,” 2019 International Conference on Innovative Trends in Computer Engineering (ITCE), Feb. 2019.
[51] S. Li, F. Cheng, C. Gu, S. Yu, and K. Huang, “Efficient Dual-Band Rectifier Using Stepped Impedance Stub Matching Network for Wireless Energy Harvesting,” IEEE Microwave and Wireless Components Letters, vol. 31, no. 7, pp. 921–924, Jul. 2021.
[52] H. Tafekirt, J. Pelegri-Sebastia, A. Bouajaj, and B. M. Reda, “A Sensitive Triple-Band Rectifier for Energy Harvesting Applications,” IEEE Access, vol. 8, pp. 73659–73664, 2020.
[53] N. Eltresy, D. Eisheakh, E. Abdallah, and H. Elhenawy, “RF Energy Harvesting Using Efficiency Dual Band Rectifier,” 2018 Asia-Pacific Microwave Conference (APMC), Nov. 2018.
[54] S. Muhammad, J. Jiat Tiang, S. Kin Wong, A. Iqbal, M. Alibakhshikenari, and E. Limiti, “Compact Rectifier Circuit Design for Harvesting GSM/900 Ambient Energy,” Electronics, vol. 9, no. 10, p. 1614, Oct. 2020.
[55] Y. Shi, J. Jing, Y. Fan, L. Yang, and M. Wang, “Design of a novel compact and efficient rectenna for WIFI energy harvesting,” Progress In Electromagnetics Research C, vol. 83, pp. 57–70, 2018.
[56] M. ur Rehman, W. Ahmad and W. T. Khan, "Highly efficient dual band 2.45/5.85 GHz rectifier for RF energy harvesting applications in ISM band," 2017 IEEE Asia Pacific Microwave Conference (APMC), 2017, pp. 150-153.
[57] D. H. Sadek, H. A. Shawkey, and A. A. Zekry, “Compact and High-Efficiency Rectenna for Wireless Power-Harvesting Applications,” International Journal of Antennas and Propagation, vol. 2021, pp. 1–8, Dec. 2021.
[58] S. D. Assimonis, S. Daskalakis and A. Bletsas, "Sensitive and Efficient RF Harvesting Supply for Batteryless Backscatter Sensor Networks," in IEEE Transactions on Microwave Theory and Techniques, vol. 64, no. 4, pp. 1327-1338, April 2016.
[59] R. Maher, A. Allam, H. Kanaya, and A. B. Abdelrahman, “Dualband rectenna for RF energy harvesting using metamaterial reflect array and novel matching technique,” Int. J. Electron. Commun., no. 155020, p. 155020, 2023.
[60] Y. Huang, J. Liang, Q. Wang, and T. Chen, “High-efficiency rectifying circuit for 5.8GHz wireless RF energy harvesting applications,” IEICE Electron. Express, vol. 21, no. 4, pp. 20230625–20230625, 2024.
[61] S. S. Ojha et al., “A dual ultra-wideband rectenna with a compact conical antenna for RF energy harvesting from S and C bands,” Results Eng., vol. 22, no. 102279, p. 102279, 2024.